Electrospun Vascular Graft Properties Following Femtosecond Laser Ablation

Carol H. Lee,[1] Yong C. Lim,[2] Heather M. Powell,[1,2] Dave F. Farson,[2] John J. Lannutti[2]

[1]*Department of Biomedical Engineering, The Ohio State University, Columbus, Ohio 43210*
[2]*Department of Materials Science and Engineering, The Ohio State University, Columbus, Ohio 43210*

Received 1 September 2010; accepted 25 November 2010
DOI 10.1002/app.34604
Published online 2 November 2011 in Wiley Online Library (wileyonlinelibrary.com).

ABSTRACT: For polymers in tissue engineering to reach their full potential, the three-dimensional integration of cells with scaffolds must become more complex. In vascular grafts this is particularly challenging as specific physical property requirements must be met. We apply a combination of polymer processing techniques—electrospinning and femtosecond laser ablation—to produce microchannels inside the walls of electrospun tubes providing for spatially-controlled cell seeding. To determine if such a scaffold can provide the desired physical properties, a greater understanding of the relationship between manufacturing and mechanics is needed. As the strength of these scaffolds is an important functional component, the relative properties of single, bi- and tri-layer combinations produced using different solvents were compared. The effect of fiber layer thickness was also investigated. The thickness of the hexafluorisopropanol-derived layer dominated the overall scaffold properties regardless of the nature of the other two layers. Although laser-machined microchannels had substantial effects on single layer and some of the bilayers, in the "final" trilayer scaffold, little effect on mechanical properties was observed. The concept of "vascular wall engineering" could successfully produce trilayer composite scaffolds that maintain the targeted mechanical properties while allowing intricate, three-dimensional cell seeding. J Appl Polym Sci 124: 2513–2523, 2012

Key words: biocompatibility; bioengineering; biological applications of polymers; biomaterials; biomimetic

INTRODUCTION

Coronary vascular disease is the leading cause of death in the US. Despite many medical advances, a critical need for synthetic vasculature remains. Over 80 million American adults have at least one type of coronary vascular disease and a coronary event occurs approximately every 25 s.[1] Additionally, more than 2 million Americans undergo cardiovascular surgery each year, many requiring coronary bypass grafting.[2] A major challenge associated with standard bypass procedures is that many patients, especially the elderly, do not possess vessels healthy enough for autologous transplantation.[3] In this context synthetic, polymer-based vasculature provides a promising alternative.

The challenge in creating synthetic grafts is a result of the multiple, often conflicting requirements they must meet: biocompatibility, mechanical properties, and ease of manufacture.[4] Current synthetic, small diameter (<6 mm) coronary grafts frequently become occluded due to early thrombosis (blood clots) and late intimal hyperplasia (thickening of the inner wall of the vessel).[5] To prevent thrombosis and hyperplasia, a human endothelial layer can be formed on the luminal surface of the synthetic graft via inoculation of endothelial cells.[6] To possess the proper strength of adhesion and function, these cells must be grown on a substrate that inherently favors adhesion, organization and specific cell–cell communication. Studies have shown that the scaffolds upon which cells are seeded are the most important factor for subsequent *in vivo* success.[7]

In addition to possessing biocompatibility and antithrombogenicity, well-designed scaffolds must also meet specific mechanical requirements to be effective. The requirement of 2000 mmHg burst pressure is mandated by clinical concerns[6] as the arteries targeted for replacement typically have burst pressures above 2000 mmHg.[8] Layering cell sheets has proven successful in creating burst pressures up to 3000 mmHg along with minimal occlusions of the vessel.[9] However, this procedure requires weeks of cell culture to form the initial thin tissue sheets, followed by eight more weeks of culturing to allow sheets to adhere to each other. Thus scaffolds which promote swift cellular organization and tissue maturation would be ideal.

In recognition of the need for multiple extracellular environments and cell types to comprise such

Correspondence to: J. J. Lannutti (lannutti.1@osu.edu).
Contract grant sponsor: National Science Foundation; contract grant numbers: CMMI-0928315, EEC-0425626.

burst pressure resistant, biocompatible synthetic vessels, we utilize our previously developed expertise in both tubular electrospinning[7] and laser ablation of electrospun fiber.[10] A trilayer tissue engineered vessel mimicking the structure and the properties of the extracellular matrix found within innermost tunica intima, the middle tunica media, and the outermost tunica adventitia of a normal blood vessel is envisioned. The tunica intima would consist of a low porosity layer to promote the formation of a continuous, endothelial cell sheet lining the lumen. A high porosity layer with laser machined helical channels that allows smooth muscle cells to infiltrate the scaffold and promotes proper orientation, would be utilized to form the tunica media. Lastly, the outermost layer would provide the appropriate *in vivo* mechanical properties including burst pressure and integration into the host vessel.

To construct scaffolds that form the synthetic component of such tissue engineered vessels, electrospinning was employed as a well-established method for creating tissue engineering scaffolds[11–14] and direct-write femtosecond laser ablation were used. Polycaprolactone (PCL) was chosen because its biocompatibility and slow degradation rate *in vivo* allows sustained load bearing capabilities.[15] Additionally, the mechanical and microstructural characteristics of PCL scaffolds can be controlled by altering the solvents in which PCL is dissolved in prior to electrospinning[16,17] and these processing variables can be exploited to create the desired trilayer construct. To produce microchannels on electrospun PCL fiber scaffolds, direct-write femtosecond laser ablation techniques were employed. Direct-write femtosecond laser ablation technique has been used only recently for microscale fabrication for biomedical applications[18] but has been shown to effectively generate linear grooves and microwells in PCL and PCL/gelatin nanofiber scaffolds.[10,19] While laser machining offers many benefits including programmable one-step processing and maintenance of sterility, the addition of laser machined microchannels in the middle layer (to assist cell infiltration) raises concerns that the strength and integrity of the resulting multilayer scaffolds could be compromised.

The final realization of this idea will allow three-dimensional integration of cells within the wall of a tubular scaffold potentially *during* a surgical intervention, thus eliminating the need for long-term cell culture. This process must also be highly predictable and reproducible. From a manufacturing viewpoint, this is challenging as the physical and biological properties of the ideal product will vary across the few hundred microns separating the inner and the outer walls of such tubes. These new capabilities in scaffold manufacturing require careful evaluation of the mechanical properties to ensure that these are preserved prior to the controlled integration of relevant cells. This study investigates the mechanical properties of these trilayer scaffolds. Tensile testing of these composites was performed to provide insight as to how the different electrospun layers interact with these deliberately introduced defects—and each other—by examining ultimate tensile stress, % elongation, and Young's modulus.

MATERIALS AND METHODS

Electrospun polycaprolactone

Three separate PCL solutions were prepared for electrospinning: (1) 14 wt % PCL (Aldrich, M_w = 80,000) in acetone (Sigma-Aldrich) solution was prepared by heating the solvent and polymer to 60°C with continuous stirring to dissolve the PCL; (2) 12 wt % PCL in distilled (over calcium hydride (Aldrich)) dichloromethane (Sigma-Aldrich) heated to 30°C with continuous stirring to dissolve the PCL; (3) 5 wt % PCL in 1,1,1,3,3,3-hexafluoro-2-propanol (Aldrich) prepared by continuously stirring the PCL in solvent until dissolution. Hereafter, the 14 wt % PCL electrospun spun from acetone is referred to as acetone-derived, the 12 wt % PCL electrospun from dichloromethane is referred to as DCM-derived, and the 5 wt % PCL electrospun from 1,1,1,3,3,3-hexafluoro-2-propanol is referred to as HFP-derived.

Once these solutions were cooled to room temperature, they were loaded in 60-cc plastic syringes (BD, Luer-Lok) with 20-gauge blunt tip needles (EFD) and electrospun using a syringe pump (KD Scientific) and high voltage power supplies (Glassman). Both random and aligned fibers were created by electrospinning solutions onto a rotating mandrel with a 1.98 m circumference and 7.62 cm length attached to a drill and rotated at either 75 rpm or 450 rpm—linear speeds of 2.5 or 15 m s^{-1}—to obtain random or aligned fibers, respectively. Random acetone-derived and DCM-derived fibers were also electrospun onto stationary 3 × 3 in. (7.6 × 7.6 cm^2) aluminum plates using the voltage potentials, flow rates, and source to ground (*S*-G) distances listed in Table I. The length of time used for electrospinning was decreased to 5 min for acetone-derived and 10 min for DCM-derived when electrospun onto the plate. Random fibers electrospun on the mandrel at slow speeds were then compared to the random fibers electrospun on the stationary plate to ensure similar microstructures and a lack of alignment. After electrospinning, all samples were placed in a vacuum at room temperature overnight to ensure that residual solvents were removed.[20–22]

To fully understand the behavior of the resulting trilayer structures, both single and bilayer electrospun sheets were fabricated. Bilayers were

TABLE I
Electrospinning Parameters

Solution (wt % PCL/solvent)	Voltage (kV)	Flow rate (mL h^{-1})	S-G Distance (cm)	Mandrel speed (m s^{-1})	Time (h)
14/acetone	24	16	10	2.5	1
12/DCM	23	15	20	2.5	2.5
5/HFP	25	15	20	15	5

composed of a second layer electrospun directly onto the first layer (acetone onto DCM or DCM onto HFP). To ensure that these layers did not delaminate from each other in the multilayer sheets post electrospinning, the source to ground distance[23] could be shortened to 10 cm as needed (Table I).

The effect of laser machined microchannels on mechanical properties by adding either one or five microchannels (described in the next section) into the gauge length of the DCM layer of the tensile specimens. Care was taken to avoid intersecting the edges of the gauge length to avoid edge effects. For the acetone-DCM bilayer, a DCM single layer was electrospun, tensile specimen were then cut, the microchannels were laser machined and, finally, the tensile specimen was remounted on the mandrel to electrospin the acetone layer on top of the microchannels. For the DCM-HFP bilayer and acetone-DCM-HFP trilayer, the HFP layer was first electrospun followed by DCM deposition on top of the HFP layer prior to cutting the tensile specimen. A schematic for the envisaged trilayer tensile specimen is shown in Figure 1.

Direct-write femtosecond laser ablation for microchannels

To fabricate microchannels on electrospun PCL nanofiber scaffolds, frequency doubled pulses from a mode-locked erbium-doped fiber laser intensified in a Ti:Sapphire regenerative amplifier laser (CPA2161, Clark-MXR) were used. The laser wavelength was $\lambda = 775$ nm. The maximum average output power of the laser was $P_{av} = 2.5$ W, pulse duration was $T_p = 150$ fs, pulse repetition frequency was $f_P = 3$ kHz and collimated beam diameter was 5 mm. The beam quality factors were $M^2 = 1.2$ in the vertical Y direction and $M^2 = 1.3$ in the horizontal X direction. Laser beam power was adjusted by a series of thin-film polarizing beam splitters and [1/2] waveplates. The attenuated laser beam was focused on the material with a 50× infinity corrected microscope objective lens having numerical aperture NA = 0.42 (M plan Apo NIR 50x, Mitutoyo). Attenuated average laser power was measured by a power meter (PM100, Thorlab) placed under the laser focusing lens. Sample motion and focus lens positioning was provided by a computer controlled motion system (MX80L, Parker) with 0.5 μm resolution in the X, Y, and Z axes. The system was programmed to scan the electrospun nanofiber scaffolds under the focused laser beam to ablate 1 or 5 microchannels on the prepared tensile specimen (Fig. 1).

The chosen dimensions of the microchannels were 100 μm wide, 100 μm deep and 1600 μm long. The X-Y motion system scanned the sample with linear paths at a scanning speed of 0.33 mm s^{-1} with a laser pulse energy of 3.33 μJ. To ablate to the desired width and depth of 100 μm, two layers consisting of 40 linear paths were used. After ablating the first layer, the focus position was adjusted downward by

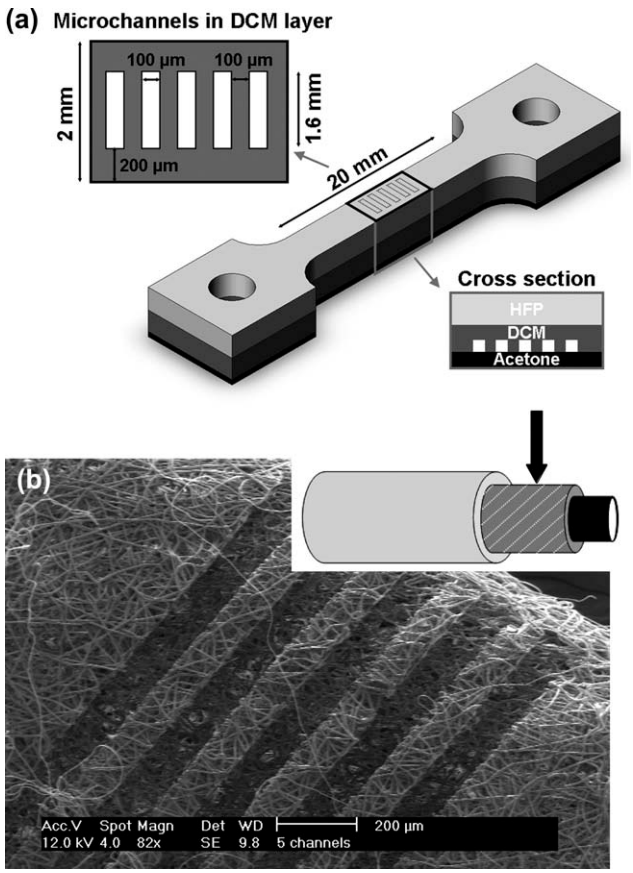

Figure 1 (a) A schematic for the desired trilayer tensile specimen with microchannels and (b) microchannels laser machined in the DCM layer as seen with SEM. The insert in (b) shows the eventual position of the laser-machined microchannels within a final tubular structure.

50 μm to ablate the second layer with the corresponding linear path spacing equal to 2.5 μm. For the 5 microchannel specimen, this process was repeated with a 100 μm spacing between microchannels (Fig. 1). This process can then be translated into a tubular format as shown in Figure 1(b) (inset).

Tensile tests

Tensile specimens were produced from as-spun polymer sheets using a 2 mm thick aluminum tensile specimen template with a 20 mm gauge length and 2.4 mm width. PCL sheets were placed in the template with fibers positioned longitudinally in the template and surgical blades (Bard-Parker No. 15) were used to cut out the straight edges of the tensile specimen, while 3 mm dermal punches (Acuderm Inc.) were used to cut the radii, ensuring that the PCL was not torn or stretched during cutting. All tensile specimen thicknesses were measured and recorded prior to tensile testing with a digital micrometer by placing the specimen between two glass microscope slides and subtracting thicknesses of the slides by the total measured thickness. The acetone layer had a thickness of 54 ± 23 μm, DCM was 223.50 ± 15.99 μm, and HFP was 113 ± 25 μm (thin HFP) or 236 ± 15 μm (thick HFP), all with a sample size (n) $\geq$ 6. Tensile data was obtained using a 222.4*N* load cell (model 31, Sensotec) and a strain rate of 2.5 mm min^{-1} on an Instron load frame (model 1322) with lightweight carbon fiber grips (A2-166 Fiber Clamp Assembly, Instron). An $n \geq 5$ was utilized for all conditions.

Some tensile curves did not display a defined failure point and instead exhibited extreme extensions of 500–700% representing the behavior of only a few fibers.[23] In these cases the % elongation was estimated based on extrapolating the slope of the first significant decrease to the point of intersection with the *x*-axis (% elongation).

Scanning electron microscopy (SEM)

The microstructure of all three component layers—including the laser machined microchannels—were observed with a SEM (XL30 ESEM) at accelerating voltages of 10–12 kV. All samples were placed on carbon tape that was applied to aluminum SEM sample mounts (SPI Supplies) and then sputter coated (Pelco Model 3 Sputter Coater 9100) with ~ 100 Å of gold over a period of 60 s using an emission current of 15 mA.

Statistical analysis

To determine the presence or absence of statistical difference between data sets, ANOVA and Tukey *t*-tests were performed using GraphPad InStat (version 3.06). *P*-values < 0.05 were considered statistically significant. All values are reported in mean ± standard deviation.

RESULTS

PCL single layers

Random acetone fibers electrospun on a mandrel rotating at 2.5 m s^{-1} were compared with those electrospun on a stationary plate, both electrospun with *S*-G distances of 10 and 20 cm. Ultimate tensile strength (UTS), % elongation, and Young's modulus (*E*) of the acetone-derived fiber either remained constant or increased when spun on a rotating mandrel (Fig. 2). The changes in UTS, *E*, and % elongation for samples electrospun at a *S-G* distance of 20 versus 10 cm were not significant although this may have partly been governed by slight variations in layer thickness. However, % elongation increased significantly when acetone-PCL was spun onto a rotating mandrel at a *S-G* distance of 10 cm (Fig. 2; $P < 0.001$).

Tensile data of single layer DCM scaffolds electrospun on the stationary plate were compared with those produced on the mandrel and no significant differences were observed (Fig. 2). However, there was a significant difference in the character of the tensile curves when comparing deposition on a plate to deposition on a mandrel. Samples from the plate failed gradually and did not exhibit a clear point of failure; in contrast, samples from the mandrel had an obvious point of failure [Fig. 3(a,b)].

The presence of microchannels in the DCM layer was examined and no statistical difference was observed in UTS and *E* for as-spun DCM without microchannels when compared with the DCM containing 1 and 5 laser machined microchannels. However a significant ($P < 0.001$) decrease in % elongation was evident with 1 and 5 microchannels (Fig. 2). The DCM tensile specimen containing one laser machined microchannel exhibited variable tensile behavior: two samples behaved similar to the original matrix without any laser machined microchannels; however, five other curves were dramatically affected by the presence of the microchannel and showed a gradual decrease in failure (Fig. 3). The graphical data showed that all samples in the 5 microchannel group exhibited failure similar to each other without the appearance of the second linear portion that occurred in all of the DCM samples without microchannels [Fig. 3(a)].

The tensile data illustrated that the thickness of the HFP layers electrospun on the mandrel at 15 m s^{-1} greatly influenced mechanical behavior. As thicknesses increase from 113 μm to 236 μm, the UTS increased by a factor of 7.5, % elongation by a

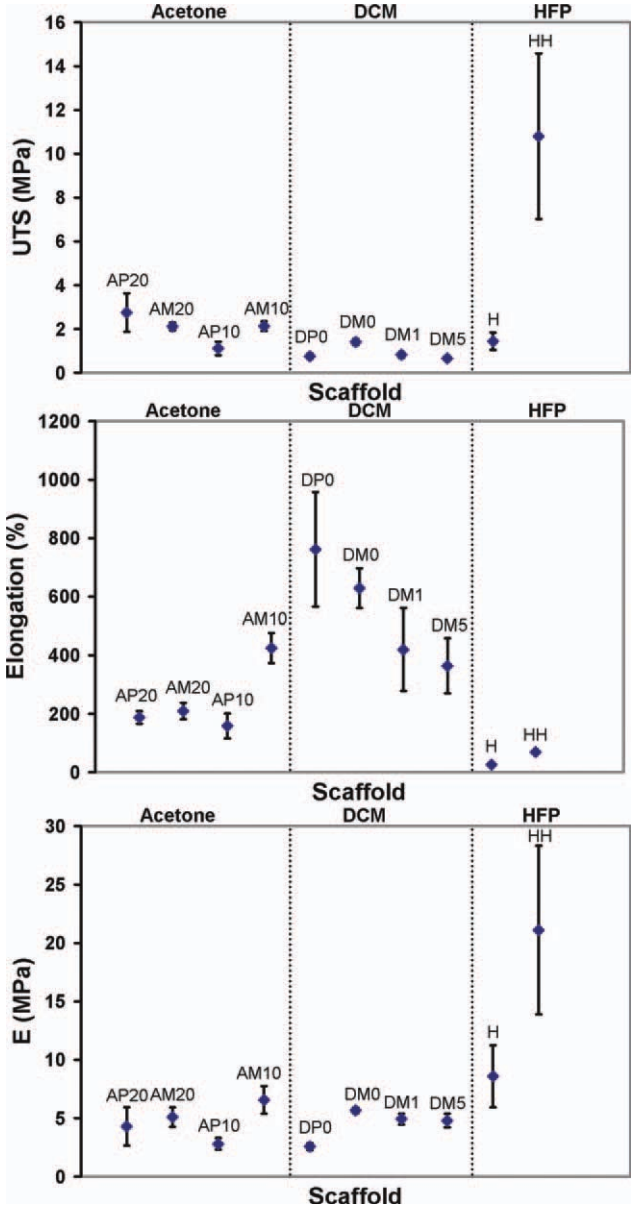

Figure 2 Mechanical properties of PCL single layers. Data points are labeled by solvent used (A, acetone; D, DCM; H, HFP), collecting ground (P, plate; M, mandrel), *S-G* distance (10 = 10 cm, 20 = 20 cm), number of channels (no channels = 0, 1 channel = 1, 5 channels = 5), and thickness of HFP for HFP layers (H, thin HFP; HH, thick HFP). For example, "AP20" = acetone fibers electrospun onto a plate with a *S-G* distance of 20 cm.

factor of 2.6, and *E* by a factor of 2.92 (Fig. 2). Tensile curves showed that failure occurred in a manner different than that of DCM samples (but similar to acetone fibers) in that the fibers failed abruptly instead of gradually (Fig. 4).

PCL bilayers

Mechanical properties of Acetone-DCM bilayers are shown in Figures 5 and 6. For the acetone and DCM bilayers, the initial use of a *S-G* distance of 20 cm[23] caused the acetone layer to delaminate from the DCM layer and resulted in consistent failure (of the acetone layer) at strains of only 137 ± 44% (Fig. 5). As this was clearly not consistent with the goal of composite behavior, the *S*-G distance was decreased to 10 cm to deliberately cause fiber–fiber bonding at the interface. This bonding was intended to avoid delamination of the acetone layer from the DCM layer. Figure 5 shows that this decrease in *S-G* distance successfully delayed failure of the acetone layer out to 336 ± 95% with little change in the final UTS, % elongation, and *E* of the remaining DCM layer.

The addition of laser machined microchannels into the DCM component of the bilayers did not significantly change UTS or *E* (Fig. 6), however, % elongation was significantly different for bilayers without microchannels versus those with either one or five microchannels. Graphically, the 1 microchannel bilayer tensile curves exhibited the same slow gradual decrease to failure seen in tensile curves for DCM single layers containing 5 microchannels. However, the samples without microchannels and those with 5 microchannels behaved differently, exhibiting an abrupt failure (Fig. 5).

Mechanical behavior was observed for HFP and DCM bilayers at two thicknesses of HFP: 113 ± 25 μm ("thin" HFP) and 236 ± 15 μm ("thick" HFP). The mechanical behavior of the thin HFP bilayers were predominantly dominated by the DCM layer as evidenced by the observation that the HFP layer failed in multiple locations along the gauge length while the DCM layer continued to experience strain. No delamination was observed between the HFP and DCM layers. Several of the bilayer samples displayed failure similar to that of DCM single layers alone, while others failed at relatively lower total elongations. The results for UTS, % elongation, and E between samples without microchannels versus with 1 or 5 microchannels were similar with no apparent statistical difference (Fig. 6).

Failure of the thick HFP-DCM bilayers was drastically different than that of the thin HFP-DCM bilayers (Fig. 6). In the absence of microchannels, the bilayer showed true composite failure originating first in the HFP layer followed by gradual extensional failure characteristic of the DCM single layer. The HFP layer first exhibited mechanical properties very similar to those of the HFP layer alone while the remaining DCM layer displays elongation statistically identical to that of DCM alone. The HFP-DCM bilayer has an UTS of 5.22 ± 0.84 MPa and *E* of 21.98 ± 2.68 MPa with HFP failure occurring at 48 ± 3%. Failure of the DCM layer occurs at 2.05 ± 0.31 MPa which is slightly higher than the DCM alone and extends to 638 ± 86% elongation. With

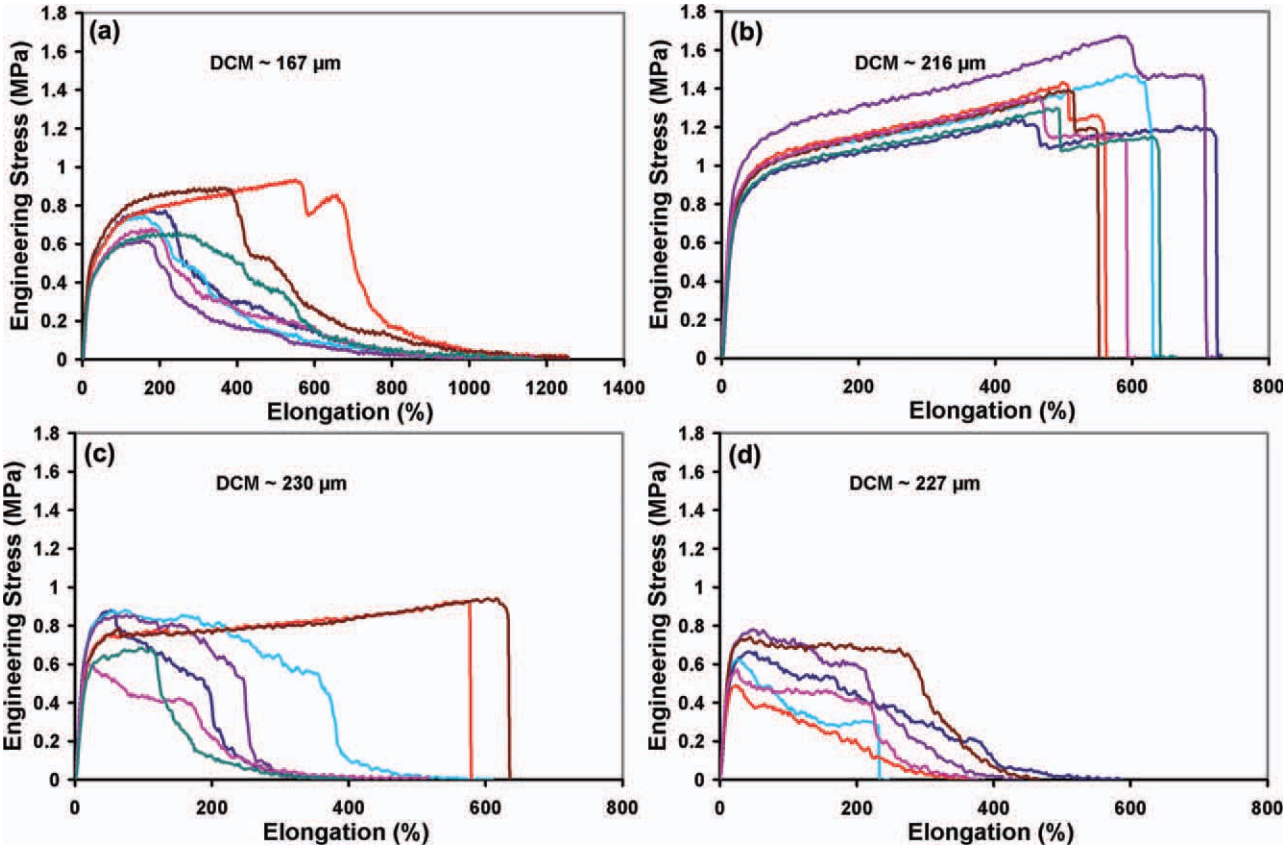

Figure 3 Failure of DCM fibers dramatically changes from (a) electrospun on a plate to electorospun on a mandrel with (b) no microchannels to (c) 1 microchannel to (d) 5 microchannels. Note that in (a) the *x*-axis extends out to 1400% elongation. [Color figure can be viewed in the online issue, which is available at wileyonlinelibrary.com.]

the addition of 1 and 5 microchannels, the bilayer mechanical behavior was surprisingly similar to that of the HFP and DCM bilayer without microchannels. Graphically, the DCM layer remaining after failure of the HFP layer was weaker than it was in the absence of microchannels. While there was no statistical difference in UTS and % elongation of the samples with 1 microchannel or 5 microchannels, there a decreasing trend of values (Fig. 6) was observed. No statistical difference was present in the % elongation for HFP, however, the % elongations for DCM were statistically different between samples without microchannels and one microchannel ($P < 0.05$) or five microchannels ($P < 0.001$) samples.

PCL trilayers

Acetone-DCM-HFP trilayers displayed a broad range of mechanical behaviors showing that the initial point of failure was statistically indistinguishable from each other in either the presence or absence of microchannels (Table II and Fig. 7). The overall behavior of the trilayers was very similar to that of the HFP-containing bilayers regardless of the presence or absence of the acetone layer. Graphically, we can observe that the presence of microchannels weakens the remaining DCM layer but this is visible only after the failure of the acetone and HFP layers (Fig. 8). As before, the HFP layer dominates the

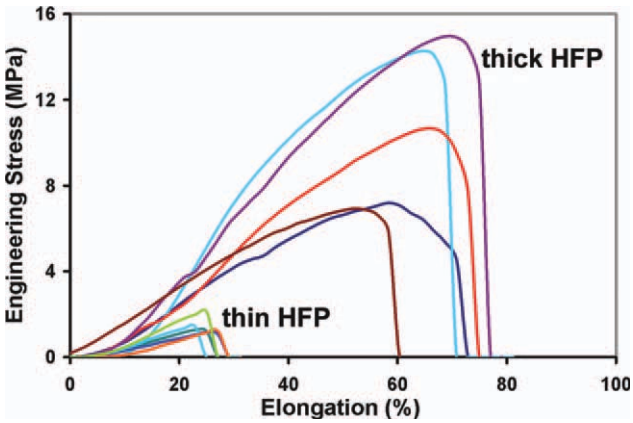

Figure 4 Thickness of the HFP layers dramatically affect mechanical properties. "Thin" (~ 113 μm) HFP layers fail before 30% elongation while "thick" (~ 236 μm) HFP fibers fail after 60% elongation. [Color figure can be viewed in the online issue, which is available at wileyonlinelibrary.com.]

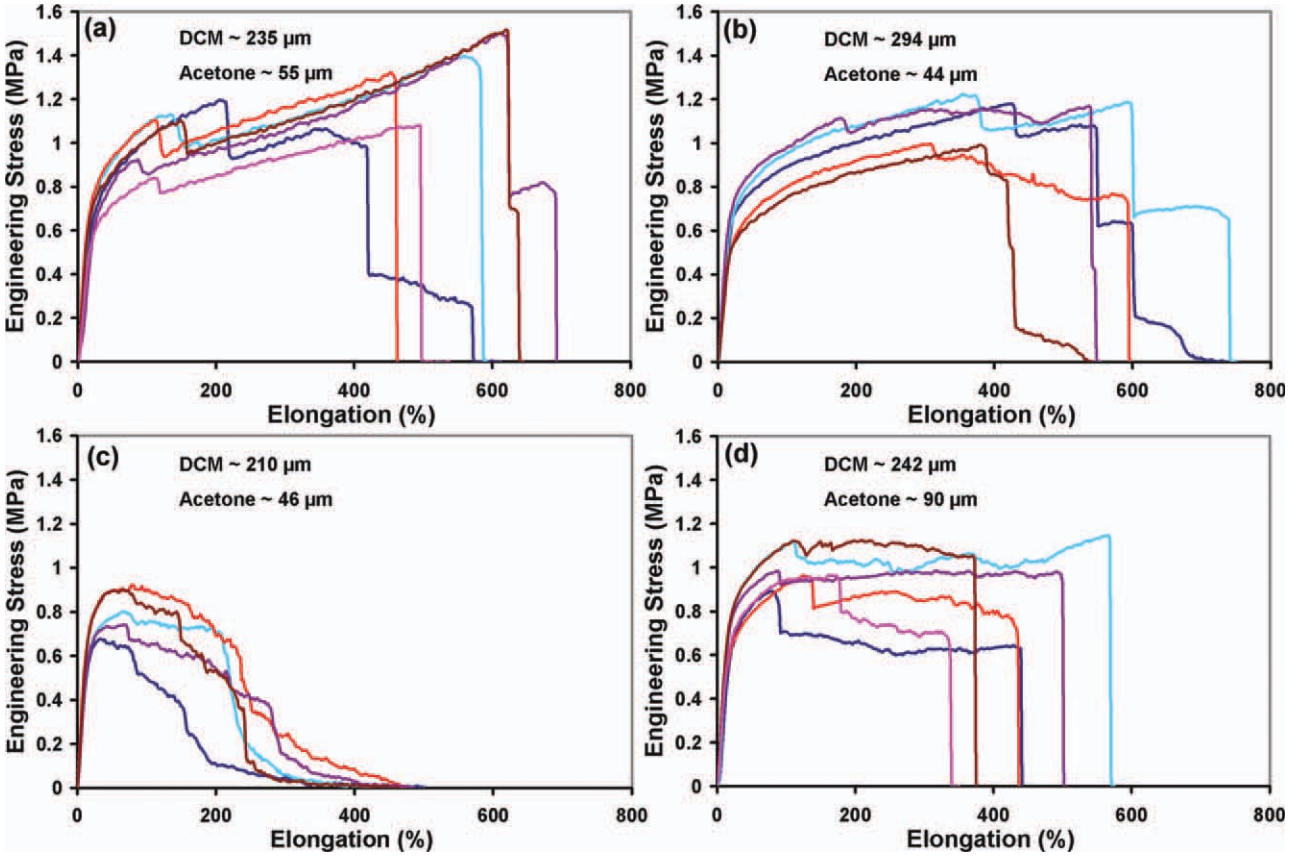

Figure 5 The acetone layer fails at larger strains when the *S*-G distance is decreased from (a) 20 cm to (b) 10 cm and the presence of (c) 1 microchannel and (b) 5 microchannels impacts fiber failure. [Color figure can be viewed in the online issue, which is available at wileyonlinelibrary.com.]

overall behavior and the effectively useful properties of these composites.

DISCUSSION

Femtosecond laser ablation is a unique tool allowing precision machining of polymer-based scaffolds, producing complex flow channel networks in electrospun scaffolds while preserving the underlying nanofiber structure.[10] By creating two- and three-dimensional patterns, favorable cell–cell interactions can be achieved. To best enable this manufacturing focus, we must develop the scientific knowledge needed to design and fabricate scaffolds with fully reproducible surface features at resolutions approaching 10 μm. The diameters and depths of desired helical passages and cavities are large compared to the diameter and the depth of material removed by a single pulse. Thus ablation must be incremental—as it is in this work—with each individual layer being "machined" by pulses of laser energy that intersect ("overlap") in the axial and circumferential motion directions as individual laser pulses (typically 20–50 μm in diameter and depth) are superimposed to produce the overall cavity. In the eventual design, helical flow channels will circle around the tube and have cross-sectional sizes of approximately 100 μm by 100 μm. Knowledge of the variation of strength in the presence of these microchannels is especially important because it can determine the size of the channels within the "tunica intima layer." The process relationships derived during this initial work provide a starting point for this process study.

PCL single layers

The changes in UTS, % elongation, and *E* observed in DCM electrospun fibers spun onto the mandrel rotating at slow speeds (2.5 m s^{-1}) versus the stationary plate are likely the result of decreased fiber–fiber bonding and slight differences in thickness (Fig. 2). No alignment of these fibers[7,23–27] was observed at these slow speeds. This comparison of deposition methods is critical to our long-term goal of fabricating tubular structures containing microchannels within the walls. To our knowledge, such tubes can only be fabricated by deposition onto a rotating mandrel. In a stationary plate, solvent

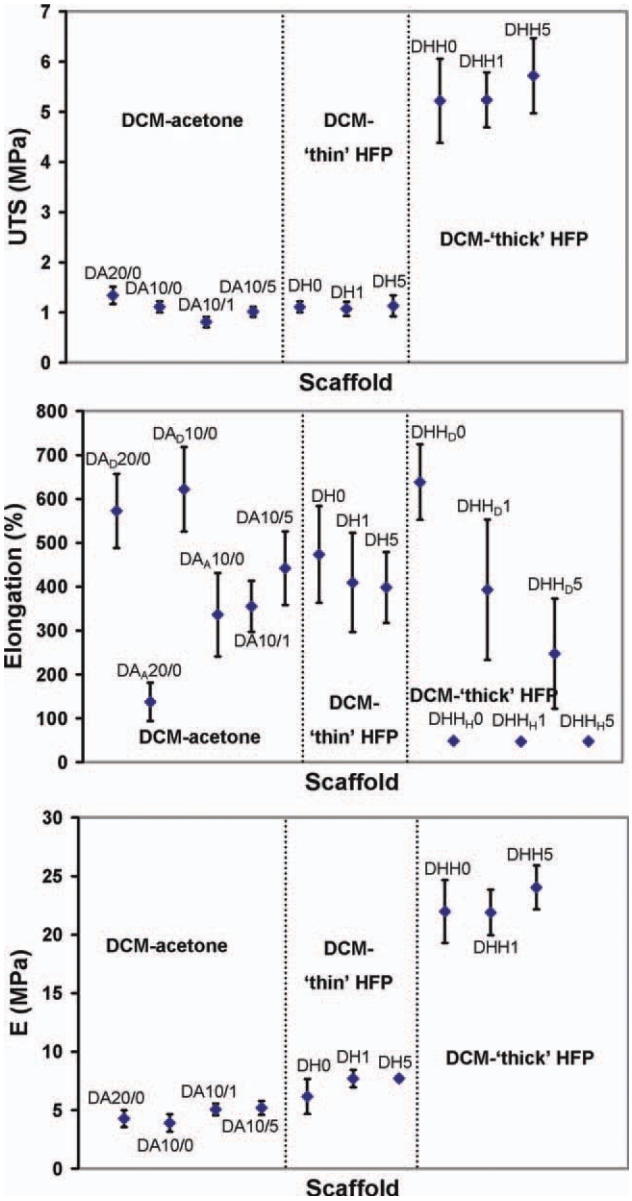

Figure 6 Mechanical properties of PCL bilayers. Data points are labeled by solvents used for layers (DA = DCM-Acetone, DH = DCM-HFP), fiber layer failure for % elongation plots ($_A$ = acetone failure, $_D$ = DCM failure, $_H$ = HFP failure), *S-G* distance (10 = 10 cm, 20 = 20 cm), thickness of HFP for HFP layers (H = thin, HH = thick), and number of channels (no channels = 0, 1 channel = 1, 5 channels = 5). For example, "DA20/0" = DCM-acetone fibers electrospun with a *S-G* of 20 cm with 0 microchannels. [Color figure can be viewed in the online issue, which is available at wileyonlinelibrary.com.]

vapors likely become trapped by successively arriving fibers during the electrospinning process and these trapped vapors can increase fiber–fiber bonding of relatively soft, as-deposited fibers. However, on a mandrel rotating at 2.5 m s^{-1}, 0.79 s separate each rotation allowing opportunities for more efficient solvent evaporation before additional fiber deposition occurs. Figure 9 shows SEM images of acetone-DCM fibers pulled to $\sim$ 80% strain demonstrating fiber–fiber bonding in fiber arrays electrospun onto the stationary plate. Elecrospun fiber arrays typically achieve larger tensile values when less fiber–fiber bonding exists because the fibers can move independently of each other.[25] The characteristic surface porosity of the DCM fibers[16,17] is also visible.

The observation of no significant differences between the tensile data for random acetone fibers with a decreased *S-G* distance of 10 cm coincides with the work of Gaumer et al. in which fibers collected on a stationary plate exhibited less differences in tensile data at *S-G* distances of 10, 15, and 20 cm.[23] Random fibers deposited on the mandrel also exhibited no significant differences in tensile data because the mandrel was rotating at a speed of only 2.5 m s^{-1}. By decreasing the *S-G* distance, more fiber–fiber bonding occurs as less time is available for the solvent to evaporate before additional fiber deposition. Fibers collected on a stationary plate follow this trend; however, those collected on the mandrel do not.

Similar to the acetone results, the UTS and *E* of DCM fibers increased when the fibers were deposited on the rotating mandrel as a result of decreased fiber–fiber bonding. The % elongation was slightly lower, but not significantly, when DCM fiber was collected on the mandrel.

With little statistical difference between the UTS and *E* of samples with and without one microchannel, electrospun DCM fibers clearly have some degree of damage tolerance. This is likely due to the fact that existing as-spun flaw sizes within these fiber arrays approach those of the microchannels; this explains the lack of sensitivity. Overall, the 1 microchannel samples behaved similarly to those fabricated without any microchannels. When 5 microchannels are ablated into the DCM fibers, decreased UTS, % elongation, and modulus were observed, implying that at some critical density these microchannels can compromise the mechanical properties of individual layers.

HFP thickness has a significant effect on mechanical properties, following the work of Drilling et al.[7] Figures 2 and 4 show UTS, % elongation, and *E* as a function of HFP thickness and these mechanical properties clearly increase as thickness increases.

PCL bilayers

Decreasing the *S-G* distance in acetone from 20 to 10 cm in the acetone and DCM bilayers showed that engineering the interface between two different fiber layers by controlling *S-G* distance offers clear benefits. The marked increase in % elongation when the *S-G* distance was decreased proved that deliberate

TABLE II
Mechanical Properties of Trilayers

HFP thickness (μm)	Channels (n)	UTS (MPa)	Elongation (%)	E (MPa)
113	0	1.02 ± 0.20	404.77 ± 83.93	5.88 ± 0.53
	1	1.18 ± 0.10	373.86 ± 153.66	7.19 ± 1.08
	5	0.94 ± 0.14	293.52 ± 172.03	5.88 ± 0.74
236	0	4.47 ± 0.64	45.40 ± 6.80 (HFP) 443.61 ± 153.96 (DCM)	18.85 ± 1.61
	1	4.94 ± 0.40	48.33 ± 4.97 (HFP) 257.85 ± 160.07 (DCM)	22.24 ± 3.11
	5	4.85 ± 0.56	47.91 ± 3.28 (HFP) 230.77 ± 152.82 (DCM)	21.93 ± 2.47

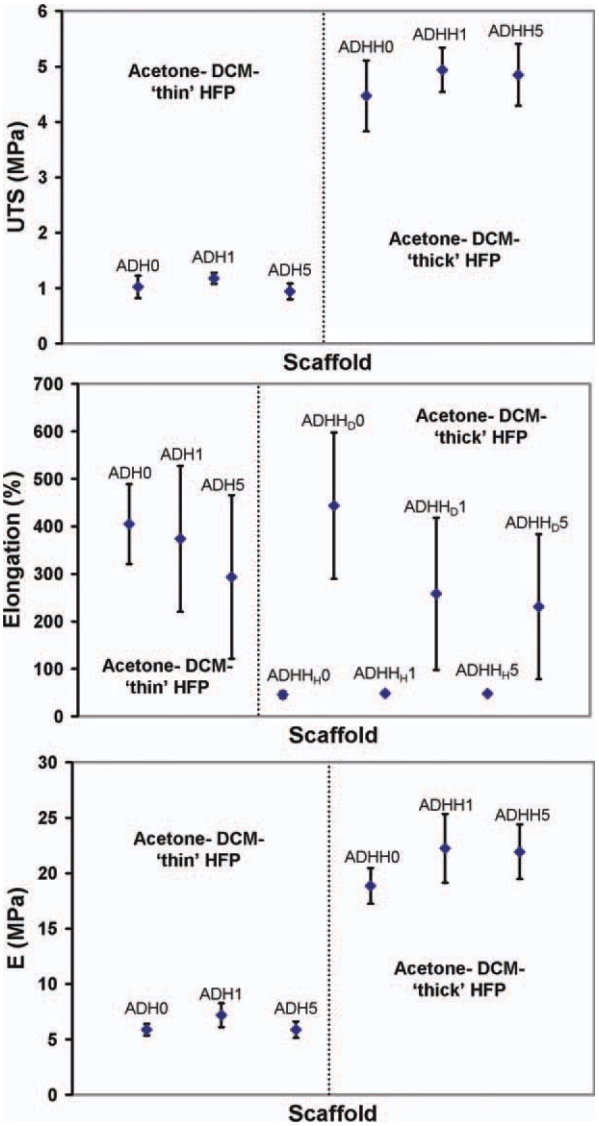

Figure 7 Mechanical properties of PCL trilayers. Data points are labeled by solvents used for layers (ADH = Acetone-DCM-HFP), fiber layer failure for % elongation plots ($_D$ = DCM failure, $_H$ = HFP failure), thickness of HFP for HFP layers (H = thin, HH = thick), and number of channels (no channels = 0, 1 channel = 1, 5 channels = 5). For example, "ADH0" = acetone-DCM-"thin" HFP trilayers with 0 microchannels. [Color figure can be viewed in the online issue, which is available at wileyonlinelibrary.com.]

fiber–fiber bonding at the interface allowed the acetone layer to better elongate in tandem with the DCM layer before failing.

Tensile data suggested that the addition of a single microchannel into the DCM component of the acetone-DCM bilayer did not greatly affect mechanical properties. This is expected as similar results were evident in DCM alone. The presence of 1 or 5 microchannels did not significantly affect the values of mechanical properties, however, graphically the

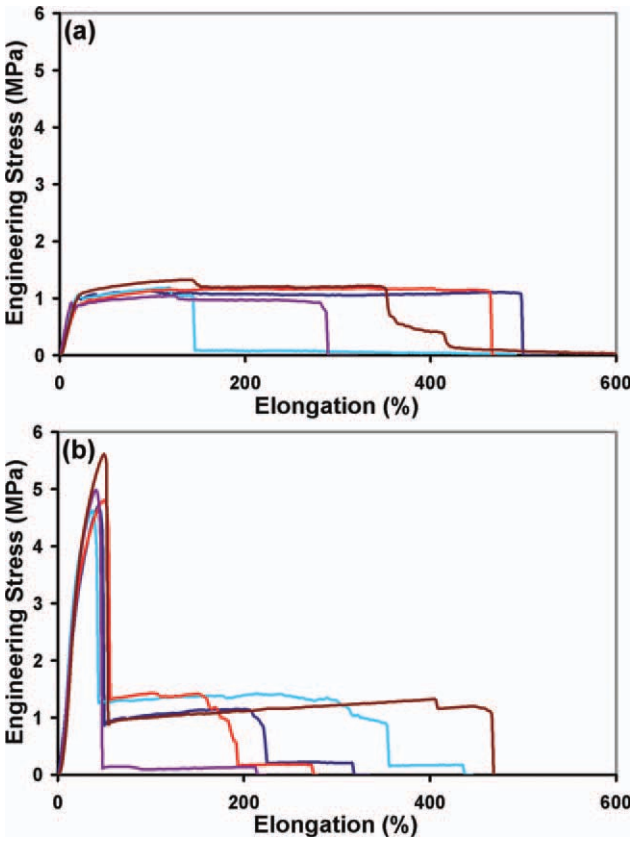

Figure 8 HFP thickness has a significant impact on the failure of these trilayers as demonstrated in (a) trilayers with "thin" HFP and (b) trilayers with "thick" HFP. [Color figure can be viewed in the online issue, which is available at wileyonlinelibrary.com.]

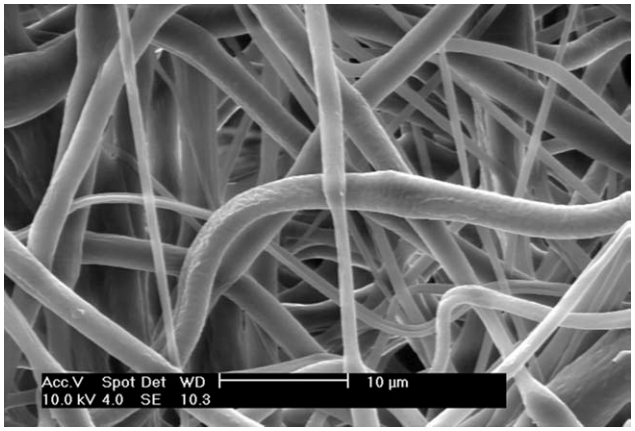

Figure 9 SEM of fiber–fiber bonding present when acetone fibers (nonporous) are electrospun onto DCM fibers (porous) on after the composite has been extended to ~ 80% strain and "frozen" into position.[7]

failure was very different between samples with 1 microchannel and samples with 5 (Fig. 5). In both cases, samples failed at a steady decline for 1 channel samples; failure occurred more abruptly for 5 channel samples. The greater resistance of the 5 channel specimens is likely due to the slightly thicker DCM layer (Fig. 5). Additionally, Figure 10 shows acetone fibers aligning when electrospun over a channel, however remaining unaligned when fiber–fiber bonded to DCM fibers. This accounts for the abrupt failure observed with 5 microchannel acetone-DCM bilayers.

For the HFP-DCM bilayers, the DCM layer dominated during strain when the HFP layer was "thin" (~ 113 μm). However, continued adherence of the HFP layer to the DCM layer even after its failure apparently served to concentrate stress in the DCM layer and led to its "early" failure. When the HFP layer was ~ 230 μm thick, the HFP dominated, providing much higher values of UTS, % elongation and modulus. This again demonstrates that thickness—a typically unappreciated variable—has dramatic effects on mechanical properties.

PCL trilayers

The addition of an acetone layer to the DCM-HFP bilayer (Fig. 7) did not compromise any of the previously observed mechanical properties of the composite electrospun bilayers (Fig. 6). In addition, the presence of microchannels also did not compromise mechanical properties of the scaffold. The DCM component of the trilayer failed earlier in the presence of microchannels; however, this was not a concern since the mechanical properties provided by the HFP were clearly sufficient to compensate for the early failure of the DCM layer.

CONCLUSIONS

Electrospun trilayer scaffolds were successfully created using acetone, DCM and HFP as the solvent for each of the three layers. Scaffolds were strained to failure to compare the relative mechanical properties of single layers, bilayers, and trilayers with and without laser ablated microchannels. Furthermore, the affect of having a "thin" versus a "thick" layer of HFP was investigated. A general theme suggests that tight control over the thickness of the individual layers will be necessary to successfully engineer load-bearing biomedical composites. Although the presence of laser machined microchannels sometimes had substantial affects on single layers and some of the bilayers investigated, in the "final" trilayer little effect on UTS, % elongation, and E was observed as the thickness of the HFP dominated the

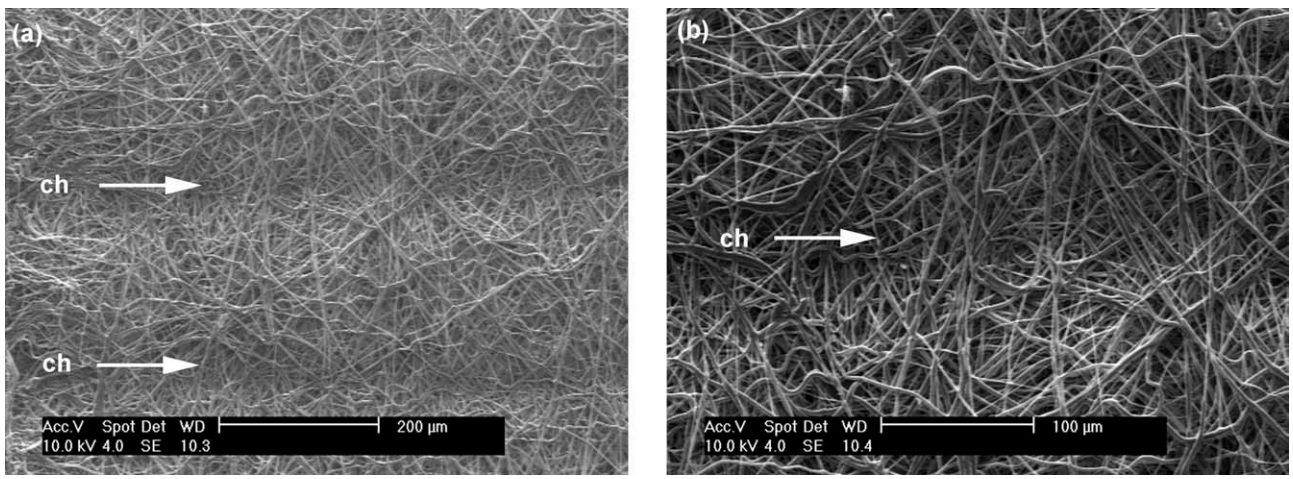

Figure 10 Acetone fibers align over microchannels in the DCM layer, but remain unaligned when bonded to the DCM fibers when the acetone layer of the acetone-DCM bilayer is strained to ~ 80%. Channels are observed as the darker horizontal bands (ch).

overall properties regardless of the nature of the other two layers. This clearly suggests that the concept of "vascular wall engineering" could potentially be successful in producing trilayer composite structures that maintain the targeted mechanical properties while allowing for subsequent cell seeding. The next step in the process is to conduct burst pressure experiments involving the final trilayer tubes to ensure that they can withstand burst pressures $>$ 2000 mmHg which should translate into the necessary *in vivo* abilities.

References

1. Lloyd-Jones, D.; Adams, R. J.; Brown, T. M.; Carnethon, M.; Dai, S.; Simone, G. D.; Ferguson, T. B.; Ford, E.; Furie, K.; Gillespie, C.; Go, A.; Greenlund, K.; Haase, N.; Hailpern, S.; Ho, P. M.; Howard, V.; Kissela, B.; Kittner, S.; Lackland, D.; Lisabeth, L.; Marelli, A.; McDermott, M. M.; Meigs, J.; Mozaffarian, D.; Mussolino, M.; Nichol, G.; Roger, V. L.; Rosamond, W.; Sacco, R.; Sorlie, P.; Stafford, R.; Thom, T.; Wasserthiel-Smoller, S.; Wong, N. D.; Wylie-Rosett, J. Circulation 2010, 121, E46.
2. Lusis, A. J. Nature 2000, 407, 233.
3. Thom, T.; Haase, N.; Rosamond, W.; Howard, V. J.; Rumsfeld, J.; Manolio, T.; Zheng, Z. J.; Flegal, K.; O'Donnell, C.; Kittner, S.; Lloyd-Jones, D.; Goff, D. C.; Hong, Y. L.; Adams, R.; Friday, G.; Furie, K.; Gorelick, P.; Kissela, B.; Marler, J.; Meigs, J.; Roger, V.; Sidney, S.; Sorlie, P.; Steinberger, J.; Wasserthiel-Smoller, S.; Wilson, M.; Wolf, P. Circulation 2006, 113, E85.
4. Isenberg, B. C.; Williams, C.; Tranquillo, R. T. Circulation Res 2006, 98, 25.
5. Walpoth, B. H.; Zammaretti, P.; Cikirikcioglu, M.; Khabiri, E.; Djebaili, M. K.; Pache, J.-C.; Tille, J.-C.; Aggoun, Y.; Morel, D.; Kalangos, A.; Hubbell, J. A.; Zisch, A. H. J Thoracic Cardiovascular Surg 2007, 133, 1163.
6. Niklason, L. E.; Gao, J.; Abbott, W. M.; Hirschi, K. K.; Houser, S.; Marini, R.; Langer, R. Science 1999, 284, 489.
7. Drilling, S.; Gaumer, J.; Lannutti, J. J Biomed Mater Res Part A 2009, 88, 923.
8. L'Heureux, N.; Dusserre, N.; Konig, G.; Victor, B.; Keire, P.; Wight, T. N.; Chronos, N. A. F.; Kyles, A. E.; Gregory, C. R.; Hoyt, G.; Robbins, R. C.; McAllister, T. N. Nat Med 2006, 12, 361.
9. L'Heureux, N.; Dusserre, N.; Marini, A.; Garrido, S.; Fuente, L. D. L.; McAllister, T. Nat Clin Practice Cardiovascular Med 2007, 4, 389.
10. Choi, H. W.; Johnson, J. K.; Nam, J.; Farson, D. F.; Lannutti, J. J. J Laser Appl 2007, 19, 225.
11. Wan, A. C. A.; Ying, J. Y. Adv Drug Deliv Rev 2010, 62, 731.
12. Agarwal, S.; Wendorff, J. H.; Greiner, A. Adv Mater 2009, 21, 3343.
13. Lannutti, J.; Reneker, D.; Ma, T.; Tomasko, D.; Farson, D. Mater Sci Eng C 2007, 27, 504.
14. Martins, A.; Araujo, J. V.; Reis, R. L.; Neves, N. M. Nanomedicine 2007, 2, 929.
15. Woodward, S. C.; Brewer, P. S.; Moatamed, F.; Schindler, A.; Pitt, C. G. J Biomed Mater Res 1985, 19, 437.
16. Nam, J.; Rath, B.; Knobloch, T. J.; Lannutti, J. J.; Agarwal, S. Tissue Eng Part A 2009, 15, 513.
17. Rath, B.; Nam, J.; Knobloch, T. J.; Lannutti, J. J.; Agarwal, S. J Biomech 2008, 41, 1095.
18. Lim, Y. C.; Altman, K. J.; Farson, D. F.; Flores, K. M. J Biomed Opt 2009, 14, 064021.
19. Lim, Y. C.; Johnson, J.; Fei, Z. Z.; Wu, Y.; Farson, D. F.; Lannutti, J.; Choi, H. W.; Lee, L. J. Biotechnol Bioeng, 2011, 108, 116.
20. Nam, J.; Huang, Y.; Agarwal, S.; Lannutti, J. J Appl Polym Sci 2008, 107, 1547.
21. Bianco, A.; Di Federico, E.; Moscatelli, I.; Camaioni, A.; Armentano, I.; Campagnolo, L.; Dottori, M.; Kenny, J. M.; Siracusa, G.; Gusmano, G. Mater Sci Eng C-Mater Biol Appl 2009, 29 2063.
22. Heath, D. E.; Lannutti, J. J.; Cooper, S. L. J Biomed Mater Res A 2010, 94, 1195.
23. Gaumer, J.; Prasad, A.; Lee, D.; Lannutti, J. Acta Biomaterialia 2009, 5, 1552.
24. Johnson, J.; Nowicki, O. M.; Lee, C. H.; Chiocca, A. E.; Viapiano, M. S.; Lawler, S. E.; Lannutti, J. J. Tissue Eng Part C 2009, 15, 531.
25. Johnson, J.; Ghosh, A.; Lannutti, J. J Appl Polym Sci 2007, 104, 2919.
26. Stella, J. A.; D'Amore, A.; Wagner, W. R.; Sacks, M. S. Acta Biomaterialia 2010, 6, 2365.
27. Edwards, M. D.; Mitchell, G. R.; Mohan, S. D.; Olley, R. H. Eur Polym J 2010, 46, 1175.